A NOTCH1-driven *MYC* enhancer promotes T cell development, transformation and acute lymphoblastic leukemia

Daniel Herranz[1], Alberto Ambesi-Impiombato[1], Teresa Palomero[1,2], Stephanie A Schnell[1], Laura Belver[1], Agnieszka A Wendorff[1], Luyao Xu[1], Mireia Castillo-Martin[3], David Llobet-Navás[3], Carlos Cordon-Cardo[3], Emmanuelle Clappier[4,5], Jean Soulier[4,5] & Adolfo A Ferrando[1,2,6]

Efforts to identify and annotate cancer driver genetic lesions have been focused primarily on the analysis of protein-coding genes; however, most genetic abnormalities found in human cancer are located in intergenic regions. Here we identify a new long range–acting *MYC* enhancer controlled by NOTCH1 that is targeted by recurrent chromosomal duplications in human T cell acute lymphoblastic leukemia (T-ALL). This highly conserved regulatory element, hereby named N-Me for NOTCH *MYC* enhancer, is located within a broad super-enhancer region +1.47 Mb from the *MYC* transcription initiating site, interacts with the *MYC* proximal promoter and induces orientation-independent *MYC* expression in reporter assays. Moreover, analysis of N-Me knockout mice demonstrates a selective and essential role of this regulatory element during thymocyte development and in *NOTCH1*-induced T-ALL. Together these results identify N-Me as a long-range oncogenic enhancer implicated directly in the pathogenesis of human leukemia and highlight the importance of the NOTCH1-MYC regulatory axis in T cell transformation and as a therapeutic target in T-ALL.

T-ALL is an aggressive hematologic malignancy resulting from the transformation of immature T cell progenitor cells[1] in which activation of transcription factor oncogenes and deregulation of transcriptional regulatory networks have particularly prominent roles[1–5]. In this context, activating mutations in *NOTCH1*, a ligand-activated transcription factor oncogene, are found in over 60% of human T-ALLs[6,7]. Mechanistically, *NOTCH1* mutations found in T-ALL result in increased NOTCH1 signaling, which promotes T cell transformation through the physiologic functions of the NOTCH1 receptor in the thymus, where ligand-induced NOTCH signaling drives hematopoietic progenitors into the T cell lineage and promotes thymocyte development[7–9]. Both the physiologic and oncogenic effects of NOTCH1 require translocation of the intracellular portion of the NOTCH1 receptor to the nucleus, where it activates gene expression in association with the recombination signal binding protein for immunoglobulin κJ region (RBPJ) DNA binding protein[7,10,11]. Gene expression studies have identified NOTCH1 as a key regulator of cell growth in T-ALL lymphoblasts directly controlling numerous genes that are involved in cell growth and metabolism[12]. The importance of understanding the hierarchy of the oncogenic NOTCH1 transcriptional programs is highlighted by the proposed role of small-molecule γ-secretase inhibitors, which block the cleavage of NOTCH1 and the release of intracellular NOTCH1 from the membrane and effectively suppress NOTCH signaling, as targeted therapies for the treatment of T-ALL[7].

Recently, numerous studies have dissected the mutational landscape of T-ALL, resulting in the identification of numerous oncogenes and tumor suppressors implicated in T cell transformation[1,4,13]. However, and most intriguingly, most genetic abnormalities found in human cancer are located in intergenic regions[14], whose role in cancer development, if any, remains poorly understood. Here we hypothesize that recurrent cancer-associated intergenic mutations, amplifications and deletions may implicate strong transcriptional regulatory sequences that are responsible for the activation of oncogenic factors downstream of key T-ALL transcription factor oncogenes such as *NOTCH1*.

RESULTS

Amplification of a *MYC* NOTCH1-occupied enhancer in T-ALL
To assess the role of intergenic copy number alterations in the pathogenesis of T-ALL, we analyzed array comparative genomic hybridization data from 160 T-ALL cases. This analysis identified recurrent focal duplications at chromosome 8q24 in 8 out of 160 (5%) cases in an area devoid of protein-coding genes located +1,427 kb downstream of *MYC* (**Fig. 1a**), a critical oncogene in the pathogenesis of NOTCH1-induced T-ALL[12,15,16] (**Fig. 1a**, **Supplementary Fig. 1** and
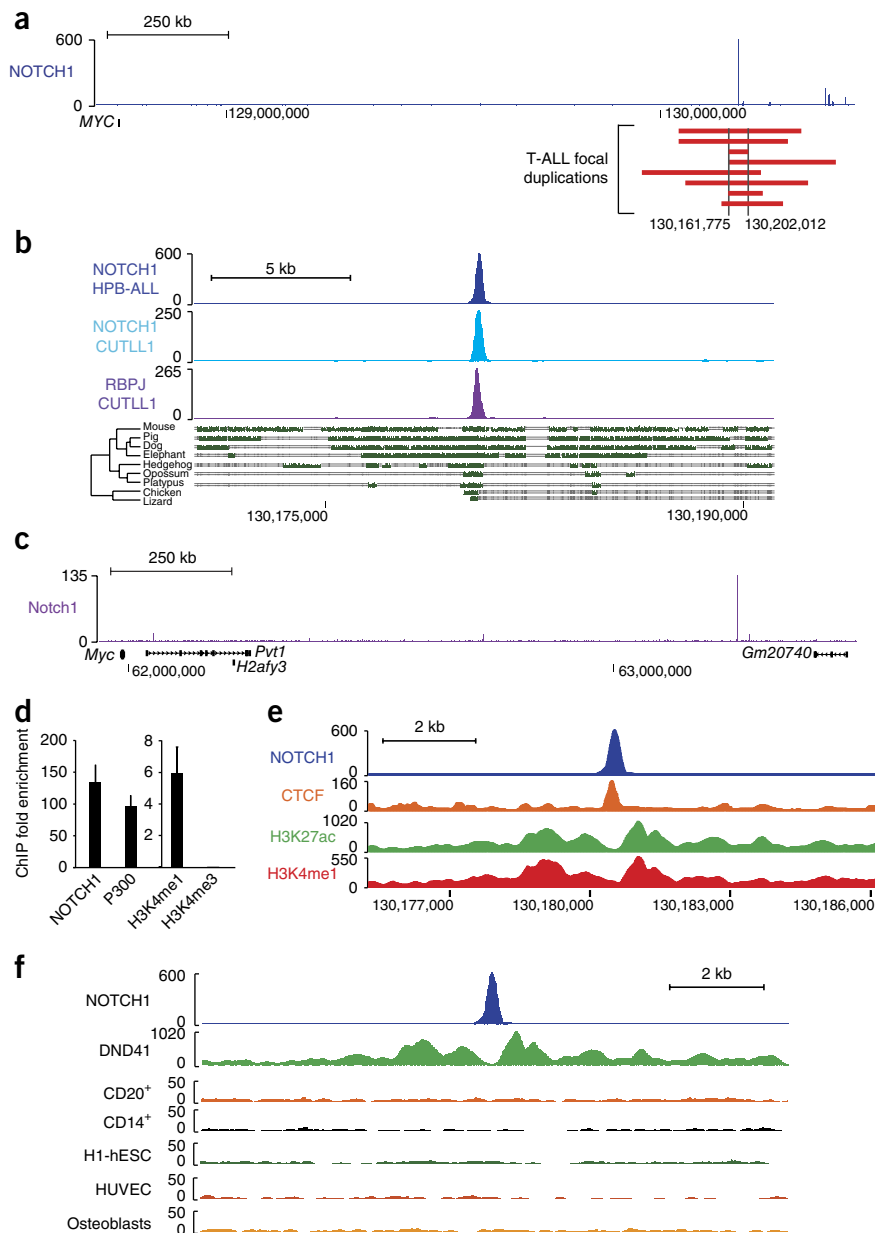
[1]Institute for Cancer Genetics, Columbia University, New York, New York, USA. [2]Department of Pathology, Columbia University Medical Center, New York, New York, USA. [3]Department of Pathology, Icahn School of Medicine at Mount Sinai, New York, New York, USA. [4]INSERM, UMR 944, Institut Universitaire d'Hématologie, Hôpital Saint-Louis, Paris, France. [5]Université Paris Diderot, Sorbonne Paris Cité, Paris, France. [6]Department of Pediatrics, Columbia University Medical Center, New York, New York, USA. Correspondence should be addressed to A.A.F. (af2196@columbia.edu).

Figure 1 Identification of N-Me, a NOTCH-bound *MYC* enhancer recurrently amplified in T-ALL. (**a**) NOTCH1 ChIP-seq binding occupancy profile in the *MYC* locus in HPB-ALL T-ALL cells and schematic representation of chromosome 8q24 focal amplifications (red bars) found in human T-ALL. (**b**) NOTCH1 and RBPJ ChIP-seq binding in T-ALL cells and multispecies sequence conservation along a 20-kb window encompassing the HPB-ALL *MYC* +1.47 Mb NOTCH1 binding site. The green blocks at the bottom represent pairwise aligned regions, with the height of the bars indicating the average base pair alignment score with the human sequence. (**c**) Notch1 ChIP-seq binding occupancy profile in the *Myc* locus in G4A2 mouse T-ALL cells. (**d**) ChIP analysis of NOTCH1, P300, H3K4me1 and H3K4me3 in HPB-ALL T-ALL cells. (**e**) CTCF (CCCTC-binding factor (zinc finger protein), a transcriptional regulator), H3K27ac and H3K4me1 ChIP-seq occupancy in DND-41 T-ALL cells along a 10-kb window containing the *MYC* +1.47 Mb NOTCH1 binding site. (**f**) ChIP-seq analysis of H3K27ac along the N-Me sequence in DND-41 T-ALL cells, B cells (CD20⁺), monocytes (CD14⁺), embryonic stem cells (H1 human embryonic stem cells, H1-hESC), endothelial cells (human umbilical vein endothelial cells, HUVEC) and osteoblasts. The *y* axes in the ChIP-seq plots indicate fragment density in counts per 10 million. The bar graphs in **d** show the mean values, and the error bars represent the s.d.

Supplementary Tables 1 and **2**). We identified no duplications in this region in 258 non–T-ALL hematologic tumors, and no germline copy number variant polymorphisms encompassing this area have been reported. Moreover, analysis of normal (remission) DNA confirmed the somatic origin of these copy number alterations in all four cases with available material (**Supplementary Fig. 1**). Notably, chromatin immunoprecipitation followed by next-generation sequencing (ChIP-seq) analysis of NOTCH1 chromatin binding sites in HPB-ALL T-ALL cells revealed a prominent 1-kb NOTCH1 peak in chromosome 8q24 located within the common 40-kb segment duplicated in T-ALL (**Fig. 1a**). A survey of NOTCH1 and RBPJ ChIP-seq data generated in the CUTLL1 T-ALL cell line[17] confirmed the presence of high levels of NOTCH1 and RBPJ binding at this site (**Fig. 1b** and **Supplementary Fig. 2**). Multispecies DNA sequence alignment revealed remarkable conservation of this region between mammals, birds and reptiles (**Fig. 1b**), with 88.6% nucleotide identity between the 500-bp human and mouse sequences centered on the NOTCH1 peak compared with an average conservation of 44% nucleotide identity along the 1.4-Mb gene desert telomeric to *MYC*. Consistently, analysis of Notch1 ChIP-seq data in G4A2 mouse T-ALL cells[18,19] revealed matching Notch1 and Rbpj binding peaks located +1,27 Mb from the *Myc* transcription initiation site (**Fig. 1c** and **Supplementary Fig. 2**).

To functionally characterize the potential role of this NOTCH1 binding site in gene regulation, we performed local ChIP analysis of chromatin regulatory factors and epigenetic histone marks in HPB-ALL T-ALL cells. These analyses confirmed high levels of NOTCH1 binding at this site and revealed *bona fide* active enhancer features associated with this region, including occupancy and high levels of P300 (also called EP300) and histone H3 Lys4 monomethylation (H3K4me1) with low levels of H3K4 trimethylation (H3K4me3) (**Fig. 1d** and **Supplementary Fig. 3**). Moreover, inspection of Encyclopedia of DNA Elements (ENCODE) data in this region revealed that this NOTCH1-occupied enhancer sits within a 20-kb segment containing high levels of H3K27 acetylation (H3K27ac) and H3K4me1 (**Fig. 1e**), features that are characteristically associated with highly dynamic long-range super-enhancer regulatory sequences[20]. In addition, extended examination of ENCODE data revealed that H3K27ac in this area is selectively present in DND-41 cells, a T-ALL cell line that harbors a highly active mutant form of *NOTCH1* (ref. 6), but not in primary CD20⁺ B cells or cell lines derived from a variety of other hematopoietic and nonhematopoietic tissues and cell lines (**Fig. 1f** and **Supplementary Fig. 3**).
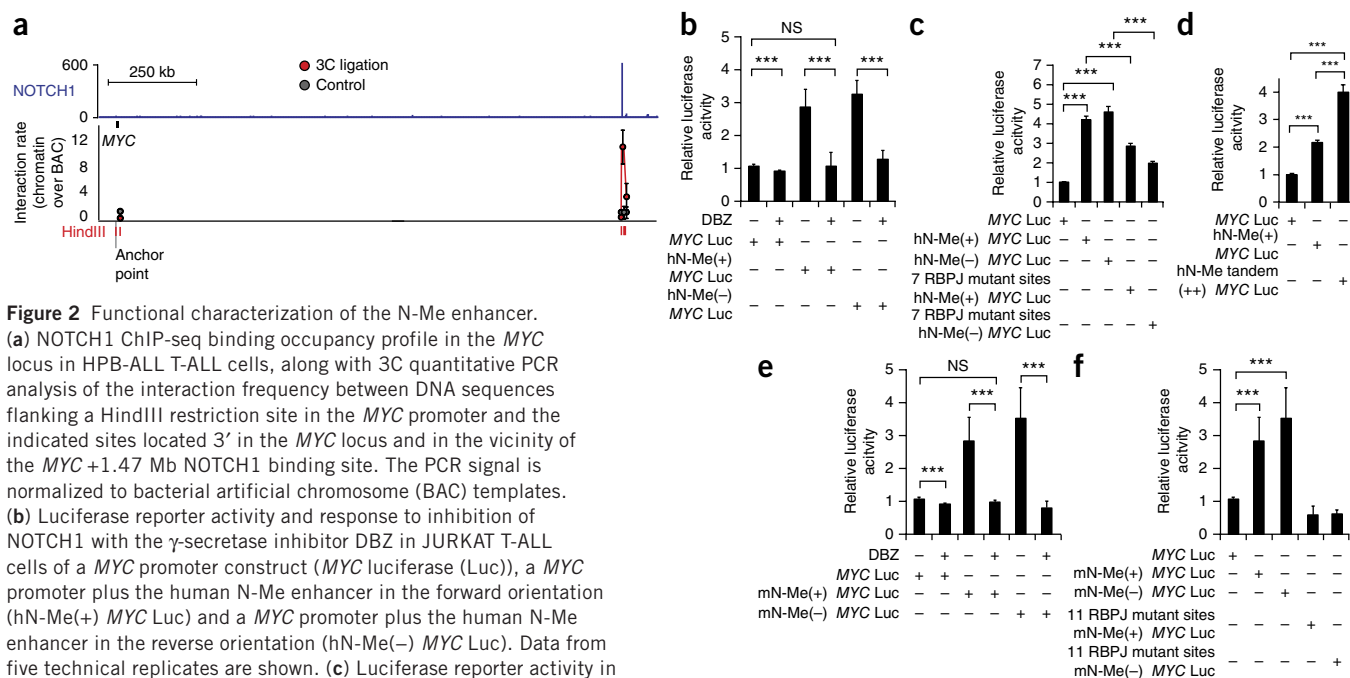
Figure 2 Functional characterization of the N-Me enhancer.
(**a**) NOTCH1 ChIP-seq binding occupancy profile in the *MYC*
locus in HPB-ALL T-ALL cells, along with 3C quantitative PCR
analysis of the interaction frequency between DNA sequences
flanking a HindIII restriction site in the *MYC* promoter and the
indicated sites located 3′ in the *MYC* locus and in the vicinity of
the *MYC* +1.47 Mb NOTCH1 binding site. The PCR signal is
normalized to bacterial artificial chromosome (BAC) templates.
(**b**) Luciferase reporter activity and response to inhibition of
NOTCH1 with the γ-secretase inhibitor DBZ in JURKAT T-ALL
cells of a *MYC* promoter construct (*MYC* luciferase (Luc)), a *MYC*
promoter plus the human N-Me enhancer in the forward orientation
(hN-Me(+) *MYC* Luc) and a *MYC* promoter plus the human N-Me
enhancer in the reverse orientation (hN-Me(−) *MYC* Luc). Data from
five technical replicates are shown. (**c**) Luciferase reporter activity in
JURKAT T-ALL cells of a *MYC* promoter construct (*MYC* Luc), a *MYC*
promoter plus the wild-type human N-Me enhancer in the forward orientation (hN-Me(+) *MYC* Luc), a *MYC* promoter plus the wild-type human N-Me
enhancer in the reverse orientation (hN-Me(−) *MYC* Luc) and both of the latter two constructs also using an hN-Me sequence with mutations in seven
RBPJ binding sites. Data from five technical replicates are shown. (**d**) Luciferase reporter activity in JURKAT T-ALL cells of a *MYC* promoter construct
(*MYC* Luc), a *MYC* promoter plus the human N-Me enhancer in the forward orientation (hN-Me(+) *MYC* Luc) and a *MYC* promoter plus a tandem
duplication of the human N-Me enhancer in the forward orientation (hN-Me tandem (++) *MYC* Luc). Data from five technical replicates are shown.
(**e**) Luciferase reporter activity and response to inhibition of NOTCH with the γ-secretase inhibitor DBZ in JURKAT T-ALL cells of a *MYC* promoter
construct (*MYC* Luc), a *MYC* promoter plus the mouse N-Me enhancer in the forward orientation (mN-Me(+) *MYC* Luc) and a *MYC* promoter plus the
mouse N-Me enhancer in the reverse orientation (mN-Me(−) *MYC* Luc). Data from five technical replicates are shown. (**f**) Luciferase reporter activity
in JURKAT T-ALL cells of a *MYC* promoter construct (*MYC* Luc), a *MYC* promoter plus the wild-type mouse N-Me enhancer in the forward orientation
(mN-Me(+) *MYC* Luc), a *MYC* promoter plus the wild-type mouse N-Me enhancer in the reverse orientation (mN-Me(−) *MYC* Luc) and both of the
latter two constructs also using a mN-Me sequence with mutations in 11 RBPJ binding sites. Data from five technical replicates are shown.
The bar graphs in **b**–**f** show the mean values, and error bars represent the s.d. *P* values were calculated using two-tailed Student's *t* test. ***$P \leq 0.005$.
NS, not significant. The *y* axes in the ChIP-seq plots indicate fragment density in counts per 10 million.

On the basis of these results, we proposed that this +1.4 Mb *MYC*
NOTCH1-occupied enhancer—hereby named N-Me for NOTCH-
bound *MYC* enhancer—could function as an important regulatory
element driving the activation of *MYC* downstream of NOTCH1 in
T-ALL. Consistent with this hypothesis, chromatin configuration
3C (chromosome conformation capture) analysis of the *MYC* locus
demonstrated the association of this enhancer with proximal regula-
tory sequences in the *MYC* promoter (**Fig. 2a**). Moreover, luciferase
reporter assays showed strong, orientation-independent activation
of reporter constructs containing this enhancer in association with
a −2.5 kb *MYC* proximal promoter[21] in JURKAT T-ALL cells, which
express high levels of constitutively active NOTCH1 protein[22], but
not in Daudi and Raji B-lineage cells (**Fig. 2b** and **Supplementary
Fig. 4**). Human N-Me–driven reporter activity in JURKAT cells was
suppressed by inhibition of NOTCH1 signaling with the γ-secretase
inhibitor DBZ and was decreased by mutation of N-Me RBPJ bind-
ing sites (**Fig. 2b,c** and **Supplementary Fig. 5**). Conversely, reporter
activity in these assays was increased by the introduction of two tan-
dem copies of the human N-Me enhancer, demonstrating a quanti-
tative, dose-dependent increase of *MYC* promoter activity by this
regulatory sequence (**Fig. 2d**). We obtained similar results in reporter
assays testing the activity and NOTCH signaling dependency of the
mouse N-Me enhancer (**Fig. 2e,f** and **Supplementary Fig. 5**). Overall
these results identify the N-Me enhancer as a recurrently duplicated

long-range regulatory element that is involved in the control of *MYC*
expression downstream of NOTCH1 in T-ALL.

The N-Me enhancer is required for thymocyte development
To test the specificity and functional relevance of the N-Me enhancer in
T cell development and transformation, we used homologous recombi-
nation in mouse embryonic stem cells to generate N-Me knockout and
conditional knockout mice (**Supplementary Fig. 6**). N-Me knockout
mice were born at Mendelian frequencies (**Supplementary Table 3**),
survived perinatally and showed normal postnatal development
without apparent behavioral abnormalities or defects in body size
(**Supplementary Fig. 7**). Notably, anatomical and histological analysis of
the mice at 6 weeks of age revealed marked selective reduction in thymus
size and cellularity in N-Me knockout animals compared to littermate
controls (**Fig. 3a–d**). Despite preservation of thymus size and architec-
ture, thymocyte counts were partially reduced in N-Me heterozygous
knockout mice (**Fig. 3a–d**). Immunohistochemical analysis of N-Me
knockout thymi showed reductions in markers of proliferation (Ki67
and phosphorylated histone H3) with no apparent increase in apopto-
sis (as assessed by cleaved caspase 3) (**Fig. 3e**). In addition, analysis of
T cell populations in the spleen and lymph nodes of N-Me knockout
animals showed a marked reduction in the number of mature CD4+ and
CD8+ T cells (**Supplementary Fig. 7**). Analysis of bone marrow hemat-
opoietic populations revealed normal numbers of B cell precursors,

Figure 3 Histological analysis of the thymus in N-Me knockout mice. (a–d) Thymus morphology (a), weight (b), cellularity (c) and histology (d) in 6-week-old wild-type (N-Me$^{+/+}$), N-Me heterozygous knockout (N-Me$^{+/-}$) and N-Me homozygous knockout (N-Me$^{-/-}$) mice ($n = 3$ per genotype). (e) Immunohistochemical analysis of Ki67, phosphorylated histone H3 (pH3) and cleaved caspase 3 expression in thymi from 6-week-old N-Me$^{+/+}$, N-Me$^{+/-}$ and N-Me$^{-/-}$ mice. Scale bars, 1 cm (a); 100 μm (d); 200 μm (e). Representative images of three independent samples are shown in d and e. The bar graphs in b and c show the mean values, and the error bars represent the s.d. P values were calculated using one-tailed Student's t test. *$P \leq 0.05$, ***$P \leq 0.005$.
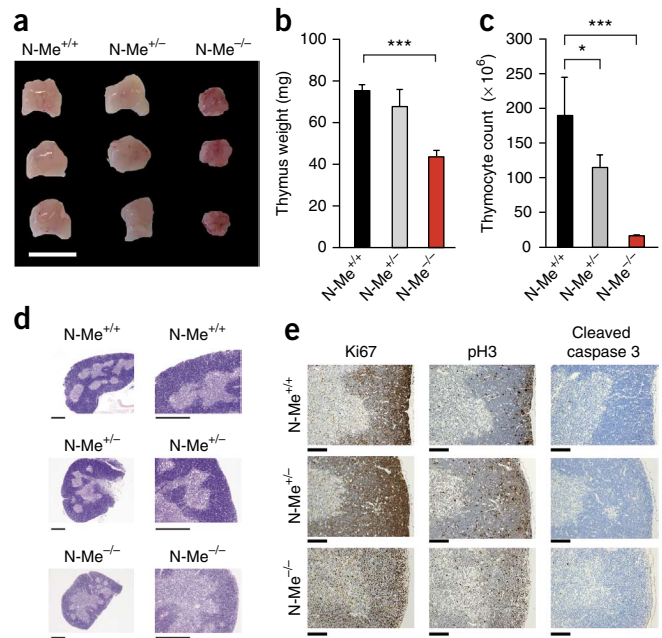
myeloid progenitors, megakaryocytes and hematopoietic stem cells (**Supplementary Fig. 7**). Moreover, histological analysis of multiple tissues, including those in which NOTCH signaling has important developmental roles, such as breast epithelium, skin and intestine, showed no alterations (**Supplementary Fig. 7**), and RT-PCR analysis showed no effects of N-Me deletion on *Myc* expression (**Supplementary Fig. 7**).

Detailed immunophenotypic analysis of thymic populations in N-Me knockout mice demonstrated accumulation of double-negative 3 (DN3, Lin$^-$CD44$^-$CD25$^+$) T cells and reductions in the numbers of CD4$^+$ and CD8$^+$ double-positive and single-positive cells (**Fig. 4a–e**). This phenotype was associated with a reduction in *Myc* expression in DN3, DN4 (Lin$^-$CD44$^-$CD25$^-$) and intermediate single-positive (ISP) cells (**Fig. 4f**). Consistently, transplantation of CD45.2 N-Me knockout bone marrow hematopoietic progenitors into lethally irradiated CD45.1 mice effectively reconstituted B cell and myeloid lineages but not T cell development (**Fig. 4g**). Moreover, retroviral expression of *MYC* in N-Me knockout hematopoietic progenitors restored their capacity to reconstitute T cell development when transplanted into immunodeficient NRG mice (**Fig. 4h**).

N-Me is required for NOTCH1-induced T cell leukemogenesis

Given the important role of NOTCH1-induced *MYC* upregulation in the pathogenesis of T-ALL, we hypothesized that deletion of the N-Me enhancer could disrupt NOTCH1-induced leukemogenesis. To test this possibility, we transplanted isogenic C57BL/6 mice with wild-type or N-Me heterozygous or homozygous knockout hematopoietic progenitors infected with retroviruses driving the expression of an
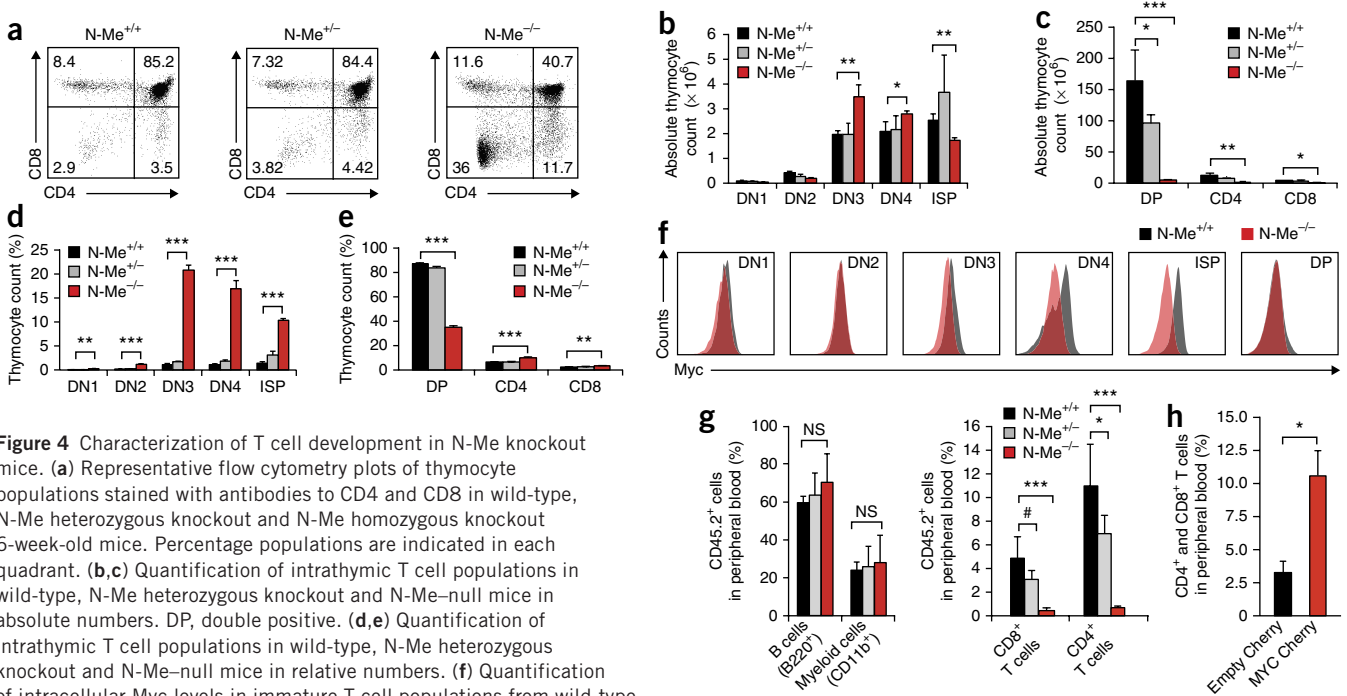

Figure 4 Characterization of T cell development in N-Me knockout mice. (a) Representative flow cytometry plots of thymocyte populations stained with antibodies to CD4 and CD8 in wild-type, N-Me heterozygous knockout and N-Me homozygous knockout 6-week-old mice. Percentage populations are indicated in each quadrant. (b,c) Quantification of intrathymic T cell populations in wild-type, N-Me heterozygous knockout and N-Me–null mice in absolute numbers. DP, double positive. (d,e) Quantification of intrathymic T cell populations in wild-type, N-Me heterozygous knockout and N-Me–null mice in relative numbers. (f) Quantification of intracellular Myc levels in immature T cell populations from wild-type and N-Me knockout mice as measured by flow cytometry. DN1, Lin$^-$CD44$^+$CD25$^-$; DN2, Lin$^-$CD44$^+$CD25$^+$. (g) Frequency of myeloid cells, B cells and T cells in the peripheral blood of CD45.1 lethally irradiated mice 6 weeks after transplantation with CD45.2 bone marrow progenitors from N-Me knockout mice. (h) Frequency of T cells in the peripheral blood of NRG mice 3 weeks after transplantation with bone marrow progenitors from N-Me knockout mice infected with retroviruses expressing mCherry (Empty Cherry) or *MYC* plus mCherry (MYC Cherry). The bar graphs in b–e, g and h show the mean values across triplicate samples, and error bars represent the s.d. P values were calculated using two-tailed Student's t test. #$P = 0.07$, *$P \leq 0.05$, **$P \leq 0.01$, *** $P \leq 0.005$. NS, not significant.
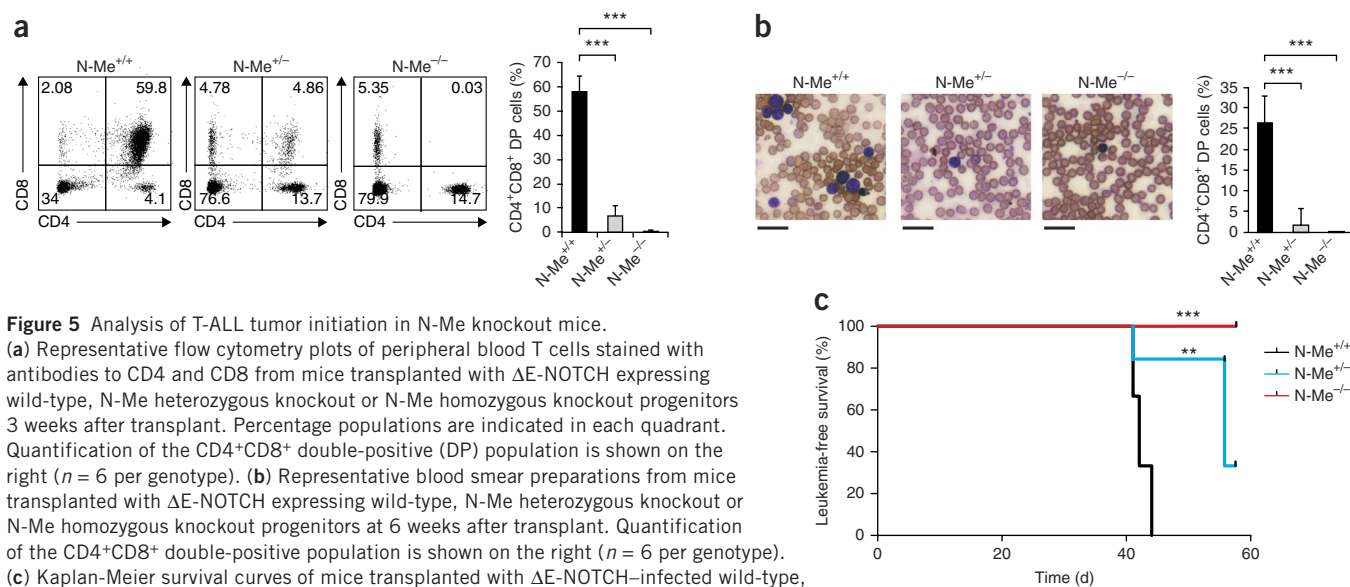
Figure 5 Analysis of T-ALL tumor initiation in N-Me knockout mice.
(**a**) Representative flow cytometry plots of peripheral blood T cells stained with antibodies to CD4 and CD8 from mice transplanted with ΔE-NOTCH expressing wild-type, N-Me heterozygous knockout or N-Me homozygous knockout progenitors 3 weeks after transplant. Percentage populations are indicated in each quadrant. Quantification of the CD4+CD8+ double-positive (DP) population is shown on the right ($n = 6$ per genotype). (**b**) Representative blood smear preparations from mice transplanted with ΔE-NOTCH expressing wild-type, N-Me heterozygous knockout or N-Me homozygous knockout progenitors at 6 weeks after transplant. Quantification of the CD4+CD8+ double-positive population is shown on the right ($n = 6$ per genotype). (**c**) Kaplan-Meier survival curves of mice transplanted with ΔE-NOTCH–infected wild-type, N-Me heterozygous knockout or N-Me homozygous knockout hematopoietic progenitors ($n = 6$ per genotype). The bar graphs in **a** and **b** show the mean values, and error bars represent the s.d. Scale bar, 100 μm (**b**). The *P* values in **a** and **b** were calculated using two-tailed Student's *t* test. ***$P \leq 0.005$. The *P* values in **c** were calculated using the log-rank test. **$P \leq 0.01$, ***$P \leq 0.005$.

oncogenic constitutively active form of NOTCH1 (ΔE-NOTCH1)[10]. Consistent with previous reports[23], mice transplanted with ΔE-NOTCH1–infected wild-type cells showed a transient early increase in the frequency of CD4+CD8+ double-positive cells in peripheral blood 3 weeks after transplant (**Fig. 5a**), which anticipated the development of overt T-ALL 3 weeks later (**Fig. 5b,c**). Mice transplanted with ΔE-NOTCH1–expressing N-Me heterozygous knockout progenitors showed a blunted increase of CD4+CD8+ double-positive cells in peripheral blood and delayed tumor development ($P < 0.01$) (**Fig. 5a–c**), whereas animals transplanted with ΔE-NOTCH1–expressing N-Me homozygous knockout cells failed to develop CD4+CD8+ double-positive cells in peripheral blood and remained leukemia free 9 weeks after transplant ($P < 0.001$) (**Fig. 5a–c**).

To explore the pathogenic role of N-Me–mediated *Myc* expression in NOTCH1-induced leukemia tumor maintenance, we generated ΔE-NOTCH1–induced T-ALL tumors from wild-type (Rosa26TM-Cre N-Me+/+) and tamoxifen-inducible conditional heterozygous (Rosa26TM-Cre N-Meflox/+) and homozygous (Rosa26TM-Cre N-Meflox/flox) N-Me knockout hematopoietic progenitors. In these experiments, mice transplanted with ΔE-NOTCH1–expressing wild-type and tamoxifen-inducible heterozygous and homozygous conditional N-Me knockout cells developed NOTCH1-induced T-ALLs with identical kinetics and immunophenotypes (**Supplementary Fig. 8**). To test the effects of N-Me deletion in established leukemia, we then injected wild-type and tamoxifen-inducible heterozygous and homozygous conditional N-Me knockout T-ALL lymphoblasts into secondary recipients and treated them with vehicle only or tamoxifen 3 days after transplant. In these experiments, tamoxifen-induced activation of Cre recombinase had no effect on leukemia progression in mice harboring wild-type tumor cells compared with controls (**Fig. 6a**). In contrast, tamoxifen-induced deletion of one copy of the N-Me enhancer in Rosa26TM-Cre N-Meflox/+ tumors or two copies in Rosa26TM-Cre N-Meflox/flox leukemias resulted in antileukemic effects and improved survival (**Fig. 6b,c**). Analysis of Rosa26TM-Cre N-Meflox/+ tumor cells recovered during disease progression after tamoxifen treatment showed heterozygous deletion of the N-Me enhancer (**Supplementary Fig. 9**), whereas analysis of tamoxifen-treated

progressing Rosa26TM-Cre N-Meflox/flox tumors demonstrated retention of one (2/9) or both (5/9) copies of the N-Meflox allele (**Supplementary Fig. 9**). We then performed limited dilution transplantations of conditional NOTCH1-induced N-Me knockout tumor cells and analyzed the effects N-Me inactivation by tamoxifen treatment on leukemia-initiating cells. In this experiment, genetic inactivation of the N-Me enhancer resulted in an ~170-fold reduction in the frequency of leukemia-initiating cells (**Supplementary Fig. 10**). Overall, these results show a strong dose-dependent effect of the N-Me enhancer in NOTCH1-induced tumor initiation and maintenance and in leukemia-initiating cell activity.

To better assess the mechanisms mediating the antileukemic effects of N-Me inactivation, we then analyzed the cellular and transcriptional phenotypes of N-Me conditional inducible knockout T-ALL cells after tamoxifen treatment. In this setting, N-Me deletion in T-ALL cells (**Supplementary Fig. 11**) resulted in unloading of RNA polymerase II (Pol II) from the *Myc* transcription start site (**Fig. 6d**) and markedly reduced *Myc* RNA and protein expression levels (**Fig. 6e,f**). At the cellular level, N-Me inactivation caused decreased cell proliferation with G1 cell cycle arrest (**Fig. 6g**). Notably, retroviral expression of *MYC* rescued the growth defect associated with genetic deletion of N-Me in NOTCH1-driven N-Me conditional knockout tumor cells (**Fig. 6h**). Gene expression profiling analysis showed that N-Me inactivation resulted in effective downregulation of *Myc*-induced gene expression programs (**Fig. 6i,j**) and gene expression signatures associated with cell growth and proliferation (**Supplementary Table 4**).

DISCUSSION

NOTCH1 has a central role in the pathogenesis of T-ALL[24] and drives an oncogenic transcriptional program that promotes cell growth proliferation and survival in T-ALL lymphoblasts. Importantly, the oncogenic effects of NOTCH1 are closely linked to activation of the *MYC* oncogene[12,15,16]. Thus, NOTCH1 activation upregulates *MYC* expression in T-ALL, and NOTCH1 and MYC have been shown to regulate overlapping transcriptional programs in a feed-forward loop transcriptional circuitry that amplifies the oncogenic effects of NOTCH1 (ref. 12). However, the specific mechanisms that drive *MYC*
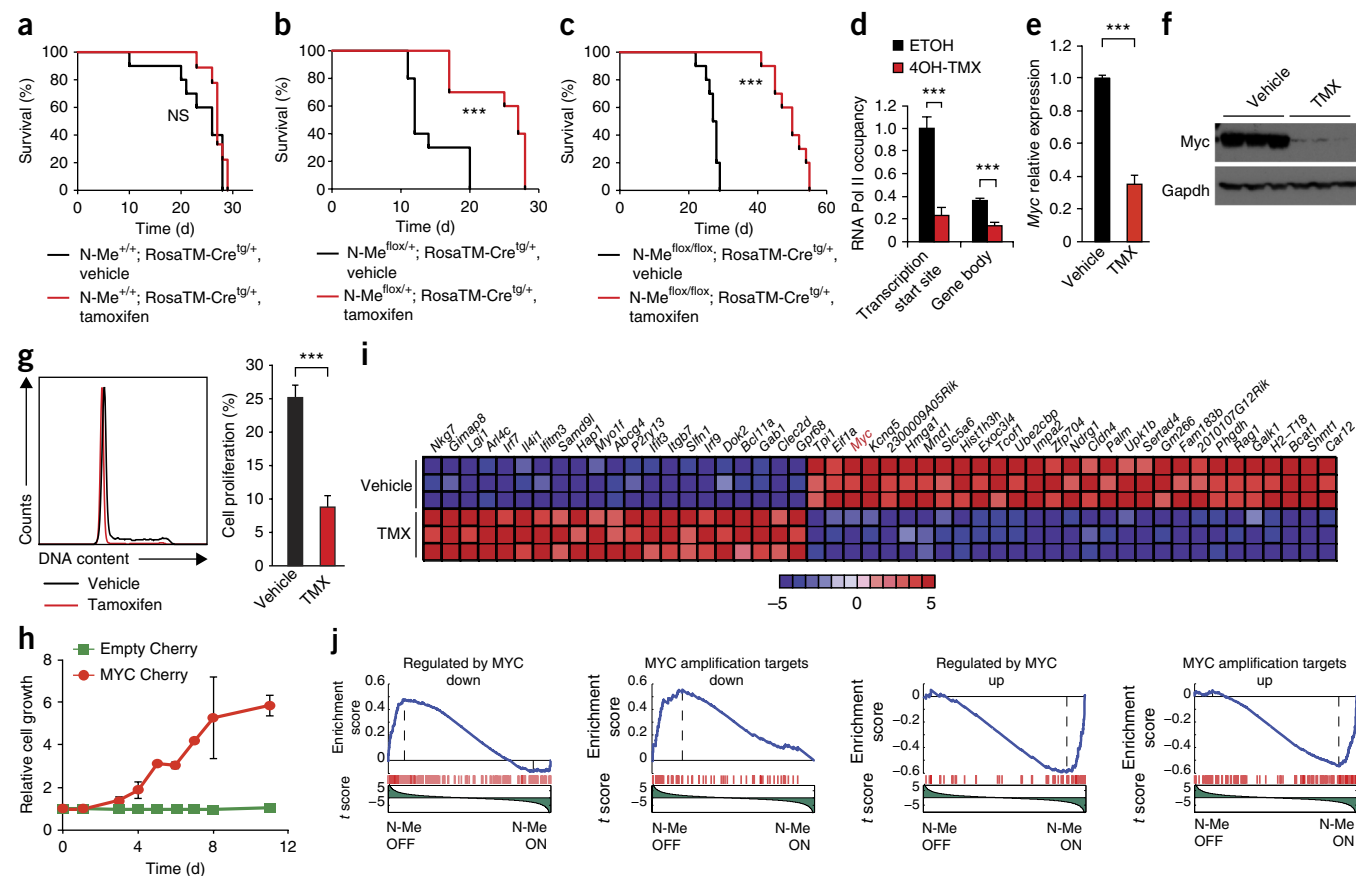
Figure 6 Analysis of leukemia maintenance in N-Me knockout cells. (**a**) Kaplan-Meier survival curves of mice harboring wild-type Rosa26TM-Cre NOTCH1-induced leukemias treated with vehicle only (*n* = 10) or tamoxifen (*n* = 9). (**b**) Kaplan-Meier survival curves of mice harboring N-Me conditional heterozygous knockout Rosa26TM-Cre NOTCH1-induced leukemias treated with vehicle only (*n* = 10) or tamoxifen (*n* = 10). (**c**) Kaplan-Meier survival curves of mice harboring N-Me conditional homozygous knockout Rosa26TM-Cre NOTCH1-induced leukemias treated with vehicle only (*n* = 10) or tamoxifen (*n* = 10). (**d**) ChIP analysis of RNA Pol II binding at the *Myc* locus 48 h after treating N-Me$^{flox/flox}$; RosaTM-Cre$^{tg/+}$ tumor cells *in vitro* with ethanol (ETOH) or 4OH-tamoxifen (4OH-TMX) to induce N-Me deletion. Data from three technical replicates are shown. (**e**) Quantitative RT-PCR analysis of *Myc* expression in tumor cells isolated from N-Me conditional knockout leukemia–bearing mice treated with vehicle only (*n* = 4) or tamoxifen (*n* = 5) *in vivo*. (**f**) Western blot analysis of *Myc* expression in tumor cells isolated from N-Me conditional knockout leukemia–bearing mice treated with vehicle only (*n* = 3) or tamoxifen (*n* = 3) *in vivo*. (**g**) Representative DNA content analysis and quantification of cell proliferation (S+G2/M fraction) of N-Me conditional knockout Rosa26TM-Cre NOTCH1-induced leukemias treated with vehicle only (*n* = 4) or tamoxifen (*n* = 5) *in vivo*. (**h**) Proliferation curve of 4OH-TMX–treated N-Me$^{flox/flox}$; RosaTM-Cre$^{tg/+}$ tumor cells infected with a murine stem cell virus (MSCV) Empty Cherry virus or an MSCV-*MYC* Cherry virus relative to ETOH-treated controls. (**i**) Heat map representation of the top 50 differentially expressed genes from Entrez Gene (*P* < 0.001) between control and tamoxifen-treated N-Me conditional knockout Rosa26TM-Cre NOTCH1-induced leukemias. The scale bar shows color-coded differential expression, with red indicating higher levels of expression and blue indicating lower levels of expression. (**j**) Gene Set Enrichment Analysis (GSEA) of genes regulated by MYC in vehicle only–treated compared to tamoxifen-treated N-Me conditional knockout Rosa26TM-Cre NOTCH1-induced leukemia cells *in vivo*. The graphs in **d**, **e**, **g** and **h** show the mean values, and the error bars represent the s.d. The *P* values in **a**–**c** were calculated using log-rank test. ****P* ≤ 0.005. NS, not significant. The *P* values in **d**, **e**, **g** and **h** were calculated using two-tailed Student's *t* test. ****P* ≤ 0.005.

expression downstream of NOTCH1 in T-ALL remain incompletely understood. Here we report the identification and functional characterization of N-Me, a T cell–specific long-range regulatory sequence driving *MYC* expression downstream of NOTCH1 in T-ALL. This regulatory element, located +1,427 kb downstream of *MYC* in humans and +1.27 kb downstream of the *Myc* locus in mice, has histone marks associated with active enhancers, interacts with *MYC* proximal regulatory sequences and sits within a broad area of H3K27ac that was characterized recently as a T cell–specific super-enhancer[25].

Transcriptional deregulation of *MYC* expression has an important role in the pathogenesis of multiple cancers, and the chromosome 8q24 region proximal to the *MYC* gene is a well-established risk locus for epithelial tumors[26–30]. Most of the genetic variants associated with cancer risk at 8q24 are located in a 500-kb gene desert

region located approximately 200 kb centromeric of the *MYC* gene. This region contains multiple enhancer regulatory sequences[31], which physically associate the *MYC* promoter using long-range chromatin loops[32]. Most notably, rs6983267, an enhancer-associated colon cancer risk allele variant in this region, has been shown to influence *MYC* expression downstream of β-catenin–transcription factor 4 (TCF4)[33]. Moreover, genetic deletion of the enhancer containing this regulatory element in the gut results in partial reduction of *Myc* expression in intestinal crypts and confers protection from intestinal tumorigenesis in *Apc*^{min} mutant mice, which develop multiple spontaneous intestinal adenomas as result of a loss-of-function mutation in the *Apc* tumor suppressor gene[34]. In contrast, no cancer-associated single-nucleotide variants have been mapped to the larger gene-free region telomeric to the *MYC* gene where N-Me resides. However, a recent report identified

a broad regulatory area of about 100 kb located 1.7 Mb telomeric to the *Myc* gene, 400 kb downstream of N-Me[35]. This *Myc* regulatory region contains multiple enhancers that are active in myeloid cells but not the thymus and is duplicated in about 3% of acute myeloid leukemias[35].

Genetic deletion of N-Me in mice resulted in reduced thymic cellularity and cell proliferation, demonstrating a critical role of this regulatory element in the homeostasis of immature T cells. N-Me–null mice showed severe reductions in the number of CD4+CD8+ double-positive cells and the subsequent single-positive CD4+ and CD8+ populations. These phenotypes recapitulate those reported in T cell–specific *Myc* conditional knockout mice (Lck-Cre *Myc*flox/flox)[36]. Given the proposed role of NOTCH1 signaling in hematopoietic stem cells and non-lymphoid tissues such as breast epithelium, we thoroughly examined a potential role for N-Me in the control of *Myc* expression in these tissues. However, consistent with a T cell–specific role of N-Me in the control of *Myc* expression, we detected no alterations in any cellular compartment other than T cells. These results suggest that NOTCH1-controlled enhancers that remain to be discovered may regulate *Myc* expression in breast epithelium and hematopoietic stem cells.

The requirement for N-Me–mediated upregulation of *Myc* expression downstream of Notch1 was even more apparent in the context of leukemia initiation, where loss of one and two copies of N-Me delayed and abrogated tumor development by oncogenic NOTCH1, respectively. In addition, N-Me was also required for the maintenance of NOTCH1-induced leukemias, as secondary deletion of one copy of N-Me in established tumors resulted in a marked delay in tumor progression, and loss of two copies effectively abrogated leukemia propagation and the self-renewal capacity of leukemia-initiating cells. These results are consistent with the well-established quantitative effects of *MYC* expression in other tumor settings. Loss of one copy of *Myc* has been shown to attenuate intestinal tumorigenesis[37], and homozygous deletion of *Myc* completely abrogates tumor development induced by loss of *Apc* in the gut[38].

Several lines of evidence support a role for loss of *Myc* expression as the primary driver in the developmental and tumor phenotypes associated with N-me loss. In this regard, we observed marked reductions in Myc expression in developing T cells from N-Me knockout mice and in T-ALL lymphoblasts after N-Me inactivation. Moreover, retroviral expression of *Myc* restored T cell lymphopoiesis from N-Me–deficient hematopoietic progenitors and rescued the defects in leukemia cell growth induced by secondary deletion on N-Me in NOTCH1-induced T-ALL cells. In addition, MYC inactivation has been associated with a global decrease in transcriptional activity, with a particularly pronounced downregulation of genes involved in growth, proliferation and metabolism[39–41], which were highly enriched in the gene expression signatures associated with N-Me loss in T-ALL.

The generation of the N-Me conditional knockout model presented here was also useful in analyzing the specific role of this enhancer in transcriptional control. Thus, even though in some cases enhancer-promoter interactions have been implicated in the regulation of transcription by promoting the release of RNA Pol II pausing[42], deletion of N-Me in T-ALL lymphoblasts resulted in unloading of RNA Pol II at the *Myc* transcription initiation site without any apparent increase in RNA Pol II pausing.

Overall, our results identify the N-Me regulatory sequence as a critical mediator of NOTCH1-induced *MYC* expression that is required for T cell development and transformation and substantiates a

pathogenic role for chromosomal duplications targeting this enhancer in the pathogenesis of T-ALL.

METHODS

1. Van Vlierberghe, P. & Ferrando, A. The molecular basis of T cell acute lymphoblastic leukemia. *J. Clin. Invest.* **122**, 3398–3406 (2012).
2. Ferrando, A.A. *et al.* Gene expression signatures define novel oncogenic pathways in T cell acute lymphoblastic leukemia. *Cancer Cell* **1**, 75–87 (2002).
3. De Keersmaecker, K. *et al.* The TLX1 oncogene drives aneuploidy in T cell transformation. *Nat. Med.* **16**, 1321–1327 (2010).
4. Della Gatta, G. *et al.* Reverse engineering of TLX oncogenic transcriptional networks identifies RUNX1 as tumor suppressor in T-ALL. *Nat. Med.* **18**, 436–440 (2012).
5. Sanda, T. *et al.* Core transcriptional regulatory circuit controlled by the TAL1 complex in human T cell acute lymphoblastic leukemia. *Cancer Cell* **22**, 209–221 (2012).
6. Weng, A.P. *et al.* Activating mutations of NOTCH1 in human T cell acute lymphoblastic leukemia. *Science* **306**, 269–271 (2004).
7. Tzoneva, G. & Ferrando, A.A. Recent advances on NOTCH signaling in T-ALL. *Curr. Top. Microbiol. Immunol.* **360**, 163–182 (2012).
8. Koch, U. & Radtke, F. Mechanisms of T cell development and transformation. *Annu. Rev. Cell Dev. Biol.* **27**, 539–562 (2011).
9. Radtke, F. *et al.* Deficient T cell fate specification in mice with an induced inactivation of Notch1. *Immunity* **10**, 547–558 (1999).
10. Schroeter, E.H., Kisslinger, J.A. & Kopan, R. Notch-1 signalling requires ligand-induced proteolytic release of intracellular domain. *Nature* **393**, 382–386 (1998).
11. Jarriault, S. *et al.* Signalling downstream of activated mammalian Notch. *Nature* **377**, 355–358 (1995).
12. Palomero, T. *et al.* NOTCH1 directly regulates c-MYC and activates a feed-forward-loop transcriptional network promoting leukemic cell growth. *Proc. Natl. Acad. Sci. USA* **103**, 18261–18266 (2006).

13. Zhang, J. *et al.* The genetic basis of early T-cell precursor acute lymphoblastic leukaemia. *Nature* **481**, 157–163 (2012).
14. Watson, I.R., Takahashi, K., Futreal, P.A. & Chin, L. Emerging patterns of somatic mutations in cancer. *Nat. Rev. Genet.* **14**, 703–718 (2013).
15. Weng, A.P. *et al.* c-Myc is an important direct target of Notch1 in T-cell acute lymphoblastic leukemia/lymphoma. *Genes Dev.* **20**, 2096–2109 (2006).
16. Sharma, V.M. *et al.* Notch1 contributes to mouse T-cell leukemia by directly inducing the expression of c-myc. *Mol. Cell. Biol.* **26**, 8022–8031 (2006).
17. Palomero, T. *et al.* CUTLL1, a novel human T-cell lymphoma cell line with t(7;9) rearrangement, aberrant NOTCH1 activation and high sensitivity to γ-secretase inhibitors. *Leukemia* **20**, 1279–1287 (2006).
18. Wang, H. *et al.* Genome-wide analysis reveals conserved and divergent features of Notch1/RBPJ binding in human and murine T-lymphoblastic leukemia cells. *Proc. Natl. Acad. Sci. USA* **108**, 14908–14913 (2011).
19. Ashworth, T.D. *et al.* Deletion-based mechanisms of Notch1 activation in T-ALL: key roles for RAG recombinase and a conserved internal translational start site in Notch1. *Blood* **116**, 5455–5464 (2010).
20. Lovén, J. *et al.* Selective inhibition of tumor oncogenes by disruption of super-enhancers. *Cell* **153**, 320–334 (2013).
21. He, T.C. *et al.* Identification of c-MYC as a target of the APC pathway. *Science* **281**, 1509–1512 (1998).
22. Sulis, M.L. *et al.* NOTCH1 extracellular juxtamembrane expansion mutations in T-ALL. *Blood* **112**, 733–740 (2008).
23. Pear, W.S. *et al.* Exclusive development of T cell neoplasms in mice transplanted with bone marrow expressing activated Notch alleles. *J. Exp. Med.* **183**, 2283–2291 (1996).
24. Ferrando, A.A. The role of NOTCH1 signaling in T-ALL. *Hematology Am. Soc. Hematol. Educ. Program* 353–361 (2009).
25. Hnisz, D. *et al.* Super-enhancers in the control of cell identity and disease. *Cell* **155**, 934–947 (2013).
26. Amundadottir, L.T. *et al.* A common variant associated with prostate cancer in European and African populations. *Nat. Genet.* **38**, 652–658 (2006).
27. Easton, D.F. *et al.* Genome-wide association study identifies novel breast cancer susceptibility loci. *Nature* **447**, 1087–1093 (2007).
28. Haiman, C.A. *et al.* Multiple regions within 8q24 independently affect risk for prostate cancer. *Nat. Genet.* **39**, 638–644 (2007).
29. Haiman, C.A. *et al.* A common genetic risk factor for colorectal and prostate cancer. *Nat. Genet.* **39**, 954–956 (2007).
30. Kiemeney, L.A. *et al.* Sequence variant on 8q24 confers susceptibility to urinary bladder cancer. *Nat. Genet.* **40**, 1307–1312 (2008).
31. Jia, L. *et al.* Functional enhancers at the gene-poor 8q24 cancer-linked locus. *PLoS Genet.* **5**, e1000597 (2009).
32. Pomerantz, M.M. *et al.* The 8q24 cancer risk variant rs6983267 shows long-range interaction with MYC in colorectal cancer. *Nat. Genet.* **41**, 882–884 (2009).
33. Wright, J.B., Brown, S.J. & Cole, M.D. Upregulation of c-MYC *in cis* through a large chromatin loop linked to a cancer risk–associated single-nucleotide polymorphism in colorectal cancer cells. *Mol. Cell. Biol.* **30**, 1411–1420 (2010).
34. Sur, I.K. *et al.* Mice lacking a Myc enhancer that includes human SNP rs6983267 are resistant to intestinal tumors. *Science* **338**, 1360–1363 (2012).
35. Shi, J. *et al.* Role of SWI/SNF in acute leukemia maintenance and enhancer-mediated Myc regulation. *Genes Dev.* **27**, 2648–2662 (2013).
36. Dose, M. *et al.* c-Myc mediates pre-TCR–induced proliferation but not developmental progression. *Blood* **108**, 2669–2677 (2006).
37. Athineos, D. & Sansom, O.J. Myc heterozygosity attenuates the phenotypes of APC deficiency in the small intestine. *Oncogene* **29**, 2585–2590 (2010).
38. Sansom, O.J. *et al.* Myc deletion rescues Apc deficiency in the small intestine. *Nature* **446**, 676–679 (2007).
39. Nie, Z. *et al.* c-Myc is a universal amplifier of expressed genes in lymphocytes and embryonic stem cells. *Cell* **151**, 68–79 (2012).
40. Lin, C.Y. *et al.* Transcriptional amplification in tumor cells with elevated c-Myc. *Cell* **151**, 56–67 (2012).
41. Lovén, J. *et al.* Revisiting global gene expression analysis. *Cell* **151**, 476–482 (2012).
42. Zippo, A. *et al.* Histone crosstalk between H3S10ph and H4K16ac generates a histone code that mediates transcription elongation. *Cell* **138**, 1122–1136 (2009).

ONLINE METHODS

Cell lines. HPB-ALL and JURKAT cells were obtained from Deutsche Sammlung von Mikroorganismen und Zellkulturen (DSMZ). Daudi and Raji cells were obtained from American Type Culture Collection. Cells were cultured in standard conditions in RPMI medium supplemented with 10% FBS and 1% penicillin-streptomycin.

NOTCH1 inhibition. We inhibited NOTCH1 in JURKAT cells with 250 nM DBZ ((S)-2-(2-(3,5-difluorophenyl)acetamido)-N-((S)-5-methyl-6-oxo-6,7-dihydro-5H-dibenzo[b,d]azepin-7-yl) propanamide) (Syncom) for 48 h as described previously[43].

Genomic analysis of primary T-ALL samples. A total of 160 cases of T-ALL from adult and pediatric patients referred to Saint-Louis Hospital, Paris, France were analyzed for copy number abnormalities using array-comparative genomic hybridization with informed consent under the supervision of the Institutional Review Board of the Institut Universitaire d'Hématologie, Université Paris-Diderot. Sureprint G3 human CGH 180K, 244K, 400K or 1M arrays (Agilent technologies) were used, and copy number alterations were identified using Genomic Workbench software and the ADM-2 algorithm (Agilent Technologies) as described previously[44].

T-ALL oncogenic subtype was determined on the basis of gene expression profiling, as reported previously[45], expression of T-ALL oncogene transcripts and the presence of specific chromosomal translocations. *NOTCH1* and *FBXW7* mutations were analyzed as described previously[46].

ChIP. We performed ChIP using the Agilent Mammalian ChIP-on-chip protocol as described previously[12,47]. Briefly, 10^8 HPB-ALL cells were fixed with formaldehyde in a final concentration of 1% for 10 min at room temperature. We quenched the crosslinking reaction with a 2.5 M glycine solution, and the cells were then centrifuged, washed once with ice-cold PBS and lysed. Cell nuclei were resuspended in lysis buffer (10 mM Tris-HCl, pH 8.0, 100 mM NaCl, 1 mM EDTA, 0.5 mM ethylene glycol tetraacetic acid (EGTA), 0.1% sodium deoxycholate and 0.5% N-lauroylsarcosine) and fragmented to a 150- to 300-bp size using a Bioruptor sonicator (Diagenode). We incubated fragmented chromatin overnight at 4 °C with magnetic beads (Dynal) loaded with 1 mg of the following specific antibodies: anti-NOTCH C-20 (sc-6014, Santa Cruz Biotechnology), anti-NOTCH1 Val1744 (2421, Cell Signaling), anti-p300 (sc-585, Santa Cruz Biotechnology), anti-H3K4me1 (ab8895, Abcam) and anti-H3K4me3 (ab1012, Abcam).

For RNA Pol II ChIP, N-Me^flox/flox; RosaTM-Cre^tg/+ tumor cells were treated *in vitro* with ethanol or tamoxifen to induce N-Me deletion. 48 h later, 10^7 cells from both conditions were processed the same way as described in the previous paragraph, and the fragmented chromatin was incubated overnight at 4 °C with magnetic beads loaded with 5 mg of the RNA Pol II antibody (sc-899, Santa Cruz Biotechnology).

We washed chromatin–antibody–bead complexes seven times with RIPA buffer (50 mM 4-(2-hydroxyethyl)-1-piperazineethanesulfonic acid (HEPES)-KOH, pH 7.6, 0.5 M LiCl, 1 mM EDTA, 1% IGEPAL (I8896, Sigma-Aldrich) and 0.7% sodium deoxycholate) and once with Tris-EDTA (TE) buffer containing 50 mM NaCl. Then we eluted the chromatin from the beads with elution buffer (50 mM Tris-HCl, pH 8.0, 10 mM EDTA and 1% SDS) and reversed the crosslink by incubation at 65 °C overnight. We purified DNA fragments with phenol-chloroform and ethanol precipitation. We tested the enrichment of specific immunoprecipitated DNA fragments by quantitative PCR as previously described[12,47].

ChIP-seq. ChIP-seq for NOTCH1 in HPB-ALL cells was performed using chromatin immunoprecipitates generated as described above and further fragmented to a 100-bp average size using a Covaris sonicator. All preparations of libraries for sequencing and the sequencing itself were performed according to the SOLiD3 System protocols. For library preparation, we performed adaptor ligation and purification, and the resulting DNA was amplified for 15 cycles. The libraries were then sequenced using 50-bp read lengths on a SOLiD3 instrument (Life Technologies).

We recovered 17,530,449 reads and 9,591,524 unique reads (defined by a unique sequencing read start site) that mapped exactly once to the hg19 human genome from the NOTCH1 ChIP-seq library, as well as 4,954,605 reads and 4,894,225 unique reads from the input control DNA library.

ChIP-seq and conservation analysis. We used the HOMER (hypergeometric optimization of motif enrichment) software suite[48] to estimate the ChIP fragment density at each position in the human genome for the HBP-ALL NOTCH1 ChIP-seq data. We also analyzed ENCODE-generated ChIP-seq data[49] and the following publicly available ChIP-seq results: CUTLL1 NOTCH1 ChIP-seq (GEO GSM732903)[18], CUTLL1 RBPJ ChIP-seq (GEO GSM732905)[18], G4A2 NOTCH1 ChIP-seq (GEO GSM732916)[18] and G4A2 RBPJ ChIP-seq (GEO GSM732917)[18].

We used the model-based analysis of ChIP-seq (MACS) algorithm[50] to call ChIP-seq peaks, and the top-scoring intergenic peak was detected at chr8:130,180,065–130,180,972 (hg19), which aligns to the mouse genome (mm10) at chr15:63,255,515–63,256,347 (80.2% of bases, 100.0% of span).

The conservation track in **Figure 1b** shows a subset of the 100 vertebrates genomic sequence alignment as produced by the UCSC Genome Browser based on the MULTIZ algorithm[51].

Quantitative 3C analysis. We performed 3C analysis of chromatin interactions as described previously[52] with some modifications. Briefly, HPB-ALL cells were crosslinked with formaldehyde in a final concentration of 1% for 10 min at room temperature. We quenched the crosslinking reaction with a 2.5 M glycine solution, and the cells were then centrifuged, washed once with ice-cold PBS and lysed. We digested cell nuclei overnight at 37 °C with the HindIII restriction enzyme. After digestion, the resulting fragments were highly diluted and ligated first for 4 h at 16 °C and then for 30 min at 37 °C. After ligation, the DNA was treated with proteinase K and de-crosslinked overnight at 65 °C. We cleaned and purified the DNA fragments by phenol-chloroform extraction and ethanol precipitation and resuspended them in 10 mM Tris, pH 7.5. The resulting 3C template was used to perform quantitative PCR using primers flanking the HindIII restriction sites located in the regions of interest within the *MYC* locus and in the vicinity of the N-Me enhancer in the 7300 quantitative PCR instrument (Applied Biosystems).

Luciferase reporter assays. We performed reporter assays using a pBV-Luc −2.5 kb *MYC* promoter luciferase construct[21] alone and coupled with upstream human and mouse N-Me enhancer sequences cloned in the forward and reverse orientations. In these assays, we electroporated in JURKAT cells with a Gene Pulser MXcell electroporator (Bio-Rad) using *MYC* luciferase reporter constructs together with a plasmid driving the expression of the *Renilla* luciferase gene (pCMV-*Renilla*) used as an internal control and treated them with DMSO or DBZ (250 nM) to inhibit NOTCH signaling. We measured luciferase activity 72 h after electroporation with the Dual-Luciferase Reporter Assay kit (Promega).

Mice and animal procedures. All animals were maintained in specific pathogen-free facilities at the Irving Cancer Research Center at Columbia University Medical Campus. Animal procedures were approved by the Columbia University Institutional Animal Care and Use Committee.

To generate N-Me conditional knockout mice, we introduced LoxP sites at mouse genomic (GRCm38/mm10) positions 63,255,283 and 63,256,404 flanking the mouse N-Me enhancer together with a neomycin selection cassette flanked by Frt sites by homologous recombination in C57BL/6 embryonic stem cells. We generated chimeras in C57BL/6 albino blastocysts using three independent targeted embryonic stem cell clones identified by PCR analysis and verified by Southern blot. We verified germline transmission in the offspring of highly chimeric male mice crossed with C57BL/6 albino females. To remove the neomycin selection cassette, we crossed mice harboring the targeting construct with a Flp germline deleter line (B6.129S4-Gt(ROSA)26Sortm1(FLP1)Dym/RainJ, the Jackson Laboratory). To generate mice carrying an N-Me deletion, we first crossed mice harboring this resulting conditional N-Me–targeted allele with a Cre germline deleter line (B6.C-Tg(CMV-*cre*)1Cgn/J, the Jackson Laboratory) and then crossed the resulting mice with wild-type C57BL/6 animals to breed out the CMV-*cre* allele. To generate conditional inducible N-Me knockout mice, we bred animals harboring the conditional N-Me targeted allele with ROSA26TM-Cre^tg/+ mice, which express a tamoxifen-inducible form of the Cre recombinase from the ubiquitous *Rosa26* locus[53].

Phenotypic characterization of N-Me knockout mice included male and female mice and isogenic age- and gender-matched controls without blinding.

For secondary deletion of N-Me using tamoxifen-induced activation of Cre recombinase, *in vivo* animals were randomly assigned to the vehicle or tamoxifen groups without blinding.

Mammary epithelial cell isolation. To determine the specific estrus stage and, thus, the concomitant mammary gland developmental phase, we analyzed female mice for the presence of leukocytes, cornified epithelial cells and nucleated epithelial cells in vaginal smears as described previously[54]. To purify mammary epithelial cells, mammary glands were dissected, mechanically disrupted and digested using a digestion solution composed by DMEM-F12, 100 units/ml penicillin-streptomycin, 2 mg/ml collagenase A and 100 units/ml hyaluronidase for 4 hours at 37 °C. After digestion, we washed the mammary epithelial cells in PBS solution and recovered them by centrifugation.

Mammary gland whole-mount preparations and carmine red staining. For whole-mount preparations, we dissected mouse mammary glands, fixed them in 4% paraformaldehyde for 1 h and stained them with carmine red (C1022, Sigma-Aldrich) overnight at room temperature. After carmine red staining, we dehydrated the stained tissues in increasing concentrations of ethanol (70, 95 and 100%) and ultimately fixed them in xylene.

Immunohistochemistry. We performed immunohistochemical stainings following standard protocols using polyclonal antibodies to Ki67 (1:1,000, 15580, Abcam), phosphorylated histone H3 (1:200, 9701, Cell Signaling Technology) and cleaved caspase 3 (1:2,000, 5AE1, Cell Signaling Technology).

Generation of NOTCH1-induced leukemias. To generate *NOTCH1*-induced T-ALL tumors in mice, we performed retroviral transduction of bone marrow cells enriched in lineage (Lin)-negative cells isolated from female mice using magnetic beads (Lineage Cell Depletion Kit, Miltenyi Biotec) with an activated form of the NOTCH1 oncogene (ΔE-NOTCH1)[10] and transplanted them by intravenous injection into lethally irradiated female isogenic recipients as described previously[55].

Flow cytometry analysis of hematopoietic populations. Single-cell suspensions of total bone marrow cells from 6-week-old wild-type and N-Me heterozygous and homozygous knockout littermates were prepared by crushing the leg bones and passing cells through a 40-µm filter. Single-cell suspensions of thymocytes were obtained by pressing one thymic lobe through a 40-µm filter. For flow cytometry–based analysis of bone marrow stem and progenitor populations and discrete stages of T cell development, cells were stained with anti-mouse fluorochrome-conjugated antibodies as follows (clone names are provided in parentheses): CD8-α phycoerythrin (PE)-Cy7 (1:800, 53-6.7), CD16/CD32 Alexa Fluor 700 (1:300, 93), CD41 PE-Cy7 (1:400, eBioMWReg30), CD44 PerCP-Cy5.5 (1:400, IM7), CD48 eFluor 450 (1:400, HM48-1), CD105 eFluor 450 (1:300, MJ7/18), CD117 PerCP-eFluor 710 (1:500, 2B8), Ly6A/E (Sca-1) PE-Cy7 (1:500, D7), biotin-CD11b (1:800, M1/70), biotin–Ly-6G (Gr1, 1:800, RB6-8C5), biotin-NK1.1 (1:800, PK136), biotin-Ter119 (1:800, TER119), biotin–CD8-α (1:800, 53-6.7), biotin-CD4 (1:800, GK1.5), biotin-CD19 (1:800, eBio1D3), biotin-CD45R (B220, 1:800, RA3-6B2) and streptavidin PE (1:400), all purchased from eBioscience. CD150 allophycocyanin (APC), CD150 PE (both 1:300, TC15-12F12.2) and Ly-6A/E (Sca-1) PE (1:300, D7) were purchased from BioLegend. CD4 APC-Cy7 (1:400, GK1.5), CD25 APC-Cy7 (1:400, PC61) and streptavidin APC-Cy7 (1:400, 554063) were purchased from BD Biosciences. Flow cytometry analysis of the different populations (hematopoietic stem cells (HSCs) and bone marrow progenitor subsets: c-Kit+Lin−Sca-1+ (KLS) total HSCs (Lin−CD117+Sca-1+), LT-HSCs (Lin−CD117+Sca-1+CD150+CD40−), ST-HSCs (Lin−CD117+Sca-1+CD150+CD40+), MPP (Lin−CD117+Sca-1+CD150−CD40+/−), CMP total (Lin−CD117+Sca-1−), CLP (Lin−CD117+Sca-1intCD135+), MkP (Lin−CD117+Sca-1−CD150+CD41+) and GMP (Lin−CD117+Sca-1−CD150−CD41−CD16/32+); T cell immature subsets in the thymus: ETP (Lin−CD117hiCD44+), DN1 (Lin−CD44+CD25−), DN2 (Lin−CD44+CD25+), DN3 (Lin−CD44−CD25+) and DN4 (Lin−CD44−CD25−)) was performed using a BD LSRII and a BD LSRFortessa cell analyzer (BD Bioscience).

For the analysis of B cell differentiation in bone marrow, we performed surface staining with the following anti-mouse fluorochrome and biotin-conjugated antibodies: B220-PE-Cy5 (1:400, RA3-6B2, BD Pharmingen), CD19-biotin (1:500, eBio1D3, eBioscience), CD25-APC-Cy7 (1:200, PC61, BD Pharmingen), IgM-APC (1:200, II/41, eBioscience) and IgD-PE (1:200, 11-26, eBioscience, 12-5993). CD19-biotin antibody was detected using PE-Cy7–conjugated streptavidin (1:500, 25-4317, eBiosciences). Flow cytometry analysis of the different populations (preproB (B220+CD19−), proB (B220+CD19+CD25−IgM−IgD−), preB (B220+CD19+CD25+IgM−IgD−) and immature B (B220+CD19+CD25−IgM+IgD−)) was performed using a FACSCanto flow cytometer (BD Bioscience).

For the analysis of T cell populations in spleen and lymph nodes, we collected tissues from 6-week-old wild-type and N-Me heterozygous and homozygous knockout littermates and processed them through a 70-µm mesh to obtain single-cell suspensions. We removed red cells in spleen samples by incubation with red blood cell lysis buffer (155 mM NH₄Cl, 12 mM KHCO₃ and 0.1 mM EDTA) for 5 min at room temperature. We stained cells with APC-conjugated antibodies against mouse CD4 (1:400, RM4-5, BD Pharmingen) and PE-conjugated antibodies against mouse CD8a (1:200, 53-6.7, BD Pharmingen).

For the analysis of megakaryocytes in bone marrow and spleen and platelets in peripheral blood, we collected tissues from 6-week-old wild-type and N-Me heterozygous and homozygous knockout littermates and processed them through a 70-µm mesh to obtain single-cell suspensions. We removed red cells samples by incubation with red blood cell lysis buffer (155 mM NH₄Cl, 12 mM KHCO₃ and 0.1 mM EDTA) for 5 min at room temperature. We stained cells with a FITC-conjugated antibody against mouse CD41 (1:200, MWReg30, eBioscience). Flow cytometry analyses were performed in a FACSCanto flow cytometer (BD Biosciences).

Bone marrow reconstitution experiments. We isolated bone marrow lineage–negative cells from N-Me+/+, N-Me+/− and N-Me−/− CD45.2-expressing mice using magnetic beads (Lineage Cell Depletion kit, Miltenyi Biotec) following the manufacturer's guidelines and then transplanted them into lethally irradiated CD45.1 C57BL/6 female mice (Taconic). 6 weeks after transplant, hematologic reconstitution of myeloid lineage, B cell lineage and T cell lineage was assessed by peripheral blood staining with the specific antibodies mentioned above and analysis in a FACSCanto flow cytometer using FACSDiva (BD Biosciences).

For the Myc rescue experiment *in vivo*, we isolated bone marrow lineage–negative cells from N-Me−/− mice as described above, infected them with either MSCV–internal ribosome entry site (IRES)-mCherry or MSCV-*MYC*-IRES-mCherry retroviruses and then transplanted them into male and female NRG (NOD.Cg-Rag1 tm1Mom Il2rg tm1Wjl/SzJ) mice (the Jackson Laboratory). We assessed T cell lineage reconstitution 3 weeks after transplant in peripheral blood by flow cytometry quantification of cells stained with specific antibodies against CD4-APC (1:400, RM4-5, BD Pharmingen) and CD8-FITC (1:200, 53-6.7, BD Pharmingen) in a BD LSRFortessa flow cytometer (BD Biosciences) using FACSDiva software (BD Biosciences).

Flow cytometry analysis of Myc expression. We collected cells from the thymi of 6-week-old male and female wild-type and N-Me knockout mice and performed surface membrane stainings using the following antibodies: CD3–Alexa Fluor 488 (1:100, 145-1211, BD Pharmingen), CD8a-PE-Cy7 (1:500, 53-6.7, eBioscience), CD44-PerCP-Cy5.5 (1:400, IM7, eBioscience), CD25-APC-Cy7 (1:200, PC61, BD Pharmingen) and CD4-APC (1:400, RM4-5, BD Pharmingen). After surface staining, we fixed the cells and permeabilized them with BD Cytofix/Cytoperm solution (BD Biosciences), washed them with BD Perm/Wash buffer (BD Biosciences) and stained them with a mouse anti-Myc antibody (1:20, 9E10, Santa Cruz) and an Alexa Fluor 546–conjugated donkey polyclonal anti-mouse IgG antibody (1:200, A10036, Invitrogen). We analyzed the intracellular levels of Myc in a FACSCanto flow cytometer (BD Biosciences) using FACSDiva software (BD Biosciences).

Microarray gene expression profiling. We isolated and snap froze spleen samples from N-Me conditional knockout NOTCH-induced T-ALL–bearing mice 40 h after treatment with vehicle only (corn oil, C8267, Sigma-Aldrich) or tamoxifen (T5648, Sigma-Aldrich; 3 mg per mouse in corn oil) administered by intraperitoneal injection. RNA was isolated, labeled and hybridized to the

doi:10.1038/nm.3665

MouseRef-8 v2.0 Expression BeadChip (Illumina) using standard procedures. Raw gene expression data were log$_2$ transformed and quantile normalized using MATLAB. Differentially expressed transcripts were identified by *t* test. Enrichment of *MYC* signature genes[56,57] was analyzed by GSEA using the *t* test metric and 10,000 permutations of the gene list[58]. Differentially expressed genes induced by tamoxifen deletion of the N-Me enhancer ($P < 0.001$, fold change >1.5) were analyzed for functional annotation enrichment using DAVID Bioinformatics web tools[59].

Quantitative real-time PCR. We performed reverse transcription reactions with the ThermoScript RT-PCR system (Invitrogen) and analyzed the resulting cDNA products by quantitative real-time PCR (FastStart Universal SYBR Green Master Mix, Roche) using a 7300 Real-Time PCR system (Applied Biosystems). Relative expression levels were normalized using *Gapdh* as a reference control.

Western blotting. Western blot analysis was performed using standard procedures. Antibodies against Myc (1:200, N-262, Santa Cruz) and Gapdh (1:10,000, D16H11, Cell Signaling) were used.

Statistical analyses. We performed statistical analyses by Student's *t* test. We assumed normality and equal distribution of variance between the different groups analyzed. Survival in mouse experiments was represented with Kaplan-Meier curves, and significance was estimated with the log-rank test (Prism GraphPad). We analyzed serial limited dilution leukemia-initiating cell data using the ELDA software[60].

43. Real, P.J. *et al.* γ-secretase inhibitors reverse glucocorticoid resistance in T cell acute lymphoblastic leukemia. *Nat. Med.* **15**, 50–58 (2009).
44. Clappier, E. *et al.* Clonal selection in xenografted human T cell acute lymphoblastic leukemia recapitulates gain of malignancy at relapse. *J. Exp. Med.* **208**, 653–661 (2011).
45. Soulier, J. *et al.* HOXA genes are included in genetic and biologic networks defining human acute T-cell leukemia (T-ALL). *Blood* **106**, 274–286 (2005).
46. Clappier, E. *et al.* NOTCH1 and FBXW7 mutations have a favorable impact on early response to treatment, but not on outcome, in children with T-cell acute lymphoblastic leukemia (T-ALL) treated on EORTC trials 58881 and 58951. *Leukemia* **24**, 2023–2031 (2010).
47. Palomero, T. *et al.* Mutational loss of PTEN induces resistance to NOTCH1 inhibition in T-cell leukemia. *Nat. Med.* **13**, 1203–1210 (2007).
48. Heinz, S. *et al.* Simple combinations of lineage-determining transcription factors prime *cis*-regulatory elements required for macrophage and B cell identities. *Mol. Cell* **38**, 576–589 (2010).
49. Encode Project Consortium. A user's guide to the encyclopedia of DNA elements (ENCODE). *PLoS Biol.* **9**, e1001046 (2011).
50. Zhang, Y. *et al.* Model-based analysis of ChIP-Seq (MACS). *Genome Biol.* **9**, R137 (2008).
51. Blanchette, M. *et al.* Aligning multiple genomic sequences with the threaded blockset aligner. *Genome Res.* **14**, 708–715 (2004).
52. Simonis, M. *et al.* High-resolution identification of balanced and complex chromosomal rearrangements by 4C technology. *Nat. Methods* **6**, 837–842 (2009).
53. Guo, K. *et al.* Disruption of peripheral leptin signaling in mice results in hyperleptinemia without associated metabolic abnormalities. *Endocrinology* **148**, 3987–3997 (2007).
54. Byers, S.L., Wiles, M.V., Dunn, S.L. & Taft, R.A. Mouse estrous cycle identification tool and images. *PLoS ONE* **7**, e35538 (2012).
55. Chiang, M.Y. *et al.* Leukemia-associated NOTCH1 alleles are weak tumor initiators but accelerate K-ras–initiated leukemia. *J. Clin. Invest.* **118**, 3181–3194 (2008).
56. Kim, Y.H. *et al.* Combined microarray analysis of small cell lung cancer reveals altered apoptotic balance and distinct expression signatures of MYC family gene amplification. *Oncogene* **25**, 130–138 (2006).
57. Zeller, K.I., Jegga, A.G., Aronow, B.J., O'Donnell, K.A. & Dang, C.V. An integrated database of genes responsive to the Myc oncogenic transcription factor: identification of direct genomic targets. *Genome Biol.* **4**, R69 (2003).
58. Subramanian, A. *et al.* Gene set enrichment analysis: a knowledge-based approach for interpreting genome-wide expression profiles. *Proc. Natl. Acad. Sci. USA* **102**, 15545–15550 (2005).
59. Huang da, W., Sherman, B.T. & Lempicki, R.A. Systematic and integrative analysis of large gene lists using DAVID bioinformatics resources. *Nat. Protoc.* **4**, 44–57 (2009).
60. Hu, Y. & Smyth, G.K. ELDA: extreme limiting dilution analysis for comparing depleted and enriched populations in stem cell and other assays. *J. Immunol. Methods* **347**, 70–78 (2009).